

Gas Accretion and Star Formation Rates[†]

Jorge Sánchez Almeida

Abstract Cosmological numerical simulations of galaxy evolution show that accretion of metal-poor gas from the cosmic web drives the star formation in galaxy disks. Unfortunately, the observational support for this theoretical prediction is still indirect, and modeling and analysis are required to identify hints as actual signs of star-formation feeding from metal-poor gas accretion. Thus, a meticulous interpretation of the observations is crucial, and this observational review begins with a simple theoretical description of the physical process and the key ingredients it involves, including the properties of the accreted gas and of the star-formation that it induces. A number of observations pointing out the connection between metal-poor gas accretion and star-formation are analyzed, specifically, the short gas consumption time-scale compared to the age of the stellar populations, the fundamental metallicity relationship, the relationship between disk morphology and gas metallicity, the existence of metallicity drops in starbursts of star-forming galaxies, the so-called G dwarf problem, the existence of a minimum metallicity for the star-forming gas in the local universe, the origin of the α -enhanced gas forming stars in the local universe, the metallicity of the quiescent BCDs, and the direct measurements of gas accretion onto galaxies. A final section discusses intrinsic difficulties to obtain direct observational evidence, and points out alternative observational pathways to further consolidate the current ideas.

Jorge Sánchez Almeida
Instituto de Astrofísica de Canarias, La Laguna, Tenerife, Spain, e-mail: jos@iac.es
Departamento de Astrofísica, Universidad de La Laguna

[†] To appear in **Gas Accretion onto Galaxies**, eds. A. J. Fox & R. Davé, 2017, Astrophysics and Space Science Library, Springer.

1 Introduction – Key physical parameters

Cosmological numerical simulations show that model galaxies tend to reach a subtle stationary state where the gas accretion rate from the cosmic web balances the star-formation rate (SFR) once outflows are taken into account (e.g., Finlator & Davé, 2008; Schaye et al., 2010; Fraternali & Tomassetti, 2012; Davé et al., 2012; Dekel et al., 2013; Bothwell et al., 2013; Feldmann, 2013; Altay et al., 2013; Forbes et al., 2014a, see also the contribution by Kereš in this Book). The balance is set because the time-scale to transform gas into stars is significantly shorter than the Hubble time and, thus, galaxies must rely on external gas accretion to maintain star-formation for a long period of time (e.g., Kennicutt, 1983; Sancisi et al., 2008, and also Sect. 3.1).

Numerical simulations reveal an intimate connection between SFR and gas accretion rate, and so, provide the rationale to study the relation observationally. In order to identify the physical parameters that have to be measured, one can resort to the toy galaxy model often referred to as bathtub model or self-regulator model. It is amply described in the literature (Tinsley, 1980; Edmunds, 1990; Bouché et al., 2010; Peeples & Shankar, 2011; Brisbin & Harwit, 2012; Davé et al., 2012; Lilly et al., 2013; Dayal et al., 2013; Dekel & Mandelker, 2014; Forbes et al., 2014b; Peng & Maiolino, 2014; Harwit & Brisbin, 2015; Rodríguez-Puebla et al., 2016; Somerville & Davé, 2015; Ascasibar et al., 2015, and also see the contribution by Lilly in this Book), and it provides the physical insight to understand the self-regulation of the star-formation (SF) process in galaxies. In this simple model, galaxies are described as structureless entities characterized by a single mass of gas M_g , a SFR, an outflow rate \dot{M}_{out} , and an inflow rate \dot{M}_{in} . We take the nomenclature and the equations from the particular implementation by Sánchez Almeida et al. (2014a). If the model galaxy is isolated and does not receive any external gas supply, then the initial mass of gas $M_g(0)$ drops exponentially in time t due to star formation (SF),

$$M_g(t) = M_g(0) \exp(-t/\tau_{in}), \quad (1)$$

with a characteristic time-scale, τ_{in} , given by,

$$\tau_{in} = \tau_g / (1 - R + \eta), \quad (2)$$

which depends on the so-called gas depletion time-scale τ_g ,

$$\tau_g = M_g / \text{SFR}, \quad (3)$$

and on the mass loading factor η ,

$$\eta = \dot{M}_{out} / \text{SFR}, \quad (4)$$

defined to be the scale factor between the SFR and the mass outflows that the SF drives. R in Eq. (2) stands for the fraction of stellar mass that returns to the interstellar medium (ISM) rather than being locked into stars and stellar remnants. If rather

than being isolated our toy galaxy is fed at a gas accretion rate $\dot{M}_{in}(t)$, then after a transient that lasts τ_{in} , it reaches a stationary state where,

$$\text{SFR}(t) = \dot{M}_{in}(t)/(1 - R + \eta). \quad (5)$$

Even if oversimplified, the above equations include all the essential ingredients giving rise to the expected relationship between gas accretion rate and SFR. Equation (5) indicates that the stationary-state SFR is set by the gas infall rate, becoming zero when the accretion rate goes to zero. Often $\eta \gg 1$, and so $\text{SFR} \ll \dot{M}_{in}$ and $\tau_{in} \ll \tau_g$. In this case, only a minor fraction of the accreted gas is used to form stars. The rest is returned unused to the circum-galactic medium (CGM) and inter-galactic medium (IGM). When this happens, the time-scale to consume the gas τ_{in} becomes much shorter than the already short gas depletion time-scale (Sect. 3.1).

Therefore, in order to provide an observational overview of the relation between gas infall rate and SFR, it is essential to keep in mind and constrain the key parameters characterizing the relation, namely, the gas depletion time-scale, the mass loading factor, and the returned mass fraction. Thus, the first section of the paper collects observational constraints on these parameters (Sect. 2). Section 3 constitutes the main body of the work, and it describes observational evidence for a relationship between SFR and metal-poor gas accretion. Unfortunately, despite the large volume of circumstantial evidence for feeding from external gas accretion, we still lack direct evidence. Several factors explain the difficulty. They are pointed out and discussed in Sects. 4 and 5, where we also mention future lines of research.

2 Characteristic physical parameters

Gas depletion time-scale τ_g . The ratio between M_g and SFR, τ_g , can be measured directly. The mass of gas and the SFR are correlated as given by the so-called Kennicutt-Schmidt relation (Schmidt, 1959; Kennicutt, 1998), which is usually formulated in terms of the gas surface density, Σ_g , and the SFR surface density, Σ_{SFR} ,

$$\Sigma_{\text{SFR}} = A \Sigma_g^N, \quad (6)$$

so that

$$\tau_g = M_g / \Sigma_{\text{SFR}} = A^{-1} \Sigma_g^{(1-N)}. \quad (7)$$

Kennicutt & Evans (2012) give A and N for disk-averaged galaxies, which lead to τ_g from 3 to 0.5 Gyr for gas surface densities between 10 and 1000 $M_\odot \text{pc}^{-2}$, typical of star-forming galaxies. Similar τ_g are obtained when considering spatially resolved measurements with sub-kpc resolution; see Fig. 1, adapted from Bigiel et al. (2008). It shows the lines of constant τ_g , and how the observations in the range of interests are close to the $\tau_g = 1$ Gyr line. The Kennicutt-Schmidt law provides an

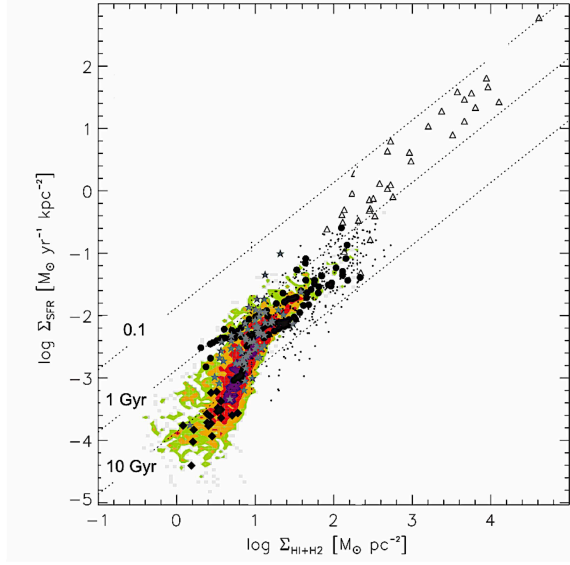


Fig. 1 Kennicutt-Schmidt relation at sub-kpc scales, i.e., SFR surface density versus gas surface density (labeled in the plot as $\Sigma_{\text{HI}+\text{H}_2} = \Sigma_g$). The slanted dotted lines represent the expected relation for constant values of τ_g of 0.1, 1, and 10 Gyr. They encompass the observed data points. Adapted from Bigiel et al. (2008, their Fig. 15).

empirical recipe linking SF with its fuel, and it has become central to the current numerical simulations of galaxy formation (e.g., Schaye & Dalla Vecchia, 2008; Dalla Vecchia & Schaye, 2008, 2012). Therefore, the relation has deserved much attention in the literature, rendering depletion time-scales in the range of the above values (see Filho et al., 2016, and references therein).

Observations suggest that τ_g decreases with increasing redshift, so that it goes from 0.5 to 2 Gyr for galaxies in the redshift range between 2 and 0 (e.g., Genzel et al., 2010; Gnedin et al., 2014). This is consistent with the theoretical expectation that τ_g scales with the instantaneous Hubble time, t_H , as $\tau_g \simeq 0.17 t_H$, so that at any time $\tau_g \ll t_H$ (Dekel et al., 2013).

Mass loading factor η . Stellar feedback is an essential ingredient of the current galaxy formation scenario since it partly controls the predicted number of low-mass galaxies. Thus, its tuning allows us to reproduce the observed galaxy mass function (e.g., Silk & Mamon, 2012; Vogelsberger et al., 2014; Schaye et al., 2015). The mass loading factor quantifies the importance of this stellar feedback (Eq. [4]). Using the toy model, it is easy to argue that w should increase with decreasing stellar mass M_* , so that for low-mass galaxies,

$$\eta \geq 1. \quad (8)$$

In the stationary state, the metallicity of the gas that forms stars, Z , is independent of SFR and M_g . Z only depends on parameters characteristic of the stellar population, and on η , explicitly,

$$Z = Z_{in} + y(1 - R)/(1 - R + \eta), \quad (9)$$

with Z_{in} the metallicity of the accreted gas, and y the stellar yield (the mass of ejected metals per unit mass locked into stars). Galaxies follow a well known mass-metallicity relation (MZR; see, e.g., Skillman et al., 1989; Tremonti et al., 2004) which, according to Eq. (9), can only be due to the dependence of η on M_* since y and R are universals given the initial mass function (IMF). Moreover, for η to modify Z in a substantial way, Eq. (8) must be satisfied.

The fact that η varies with M_* reaching large values for low-mass galaxies is found both in numerical simulations and in observational works. In order to reproduce the MZR, Peeples & Shankar (2011), Davé et al. (2012), and Dayal et al. (2013) use η varying from 1 to 6 when M_* goes from 10^{11} to $10^9 M_\odot$. The numerical simulations by Shen et al. (2012) lead to η between 1 and 10 for M_* from 2×10^{11} to $10^9 M_\odot$. In the cases modeled by Christensen et al. (2016), it goes from 0.5 to 50 for galaxies with virial masses from 10^{12} to $2 \times 10^9 M_\odot$. The numerical simulations carried out by Davé et al. (2013) assume η to be proportional to $M_*^{-1/3}$, with an even steeper dependence at low masses. The numerical simulations of giant star-forming clumps in gas-rich galaxies by Bournaud et al. (2014) render an effective η exceeding 2. Thompson & Krumholz (2016) model supersonic-turbulence driven outflows, and infer w ranging from 10^{-3} to 10. Observations of Mg II absorption around massive galaxies with $M_* \sim 10^{11} M_\odot$ are used by Bordoloi et al. (2014) to set a conservative lower limit to η , which has to be larger than 0.24. Mass loading factors observed at high redshift generally refer to massive objects ($M_* > 10^{10} M_\odot$), and turn out to be between 0.5 and 2 (Newman et al., 2012; Martin et al., 2012). It is not uncommon to infer factors up to 10 in local dwarfs (Martin, 1999; Veilleux et al., 2005). An extreme case is presented by Olmo-García et al. (2016), where faint multiple components in the wings of $H\alpha$ are interpreted as produced by SN driven outflows with η often larger than 20.

Returned fraction R . Once the IMF is set, the stellar mass returned to the ISM is provided by stellar evolution models. 10 Gyr after the starburst, R is typically in the range between 0.2 and 0.3 when a Salpeter IMF is adopted (e.g., Edmunds, 2005; Leitner & Kravtsov, 2011). It can reach 0.5 for a Kroupa IMF, that has more massive stars for the same total mass of the stellar population (e.g., Leitner & Kravtsov, 2011; Segers et al., 2016).

3 Evidence for a relationship between the SFR and the gas infall rate

3.1 The gas-consumption timescale

The time-scale to consume the gas is too short for the observed stellar ages, therefore, a continuous gas supply is needed to explain why all types of galaxies have been forming stars for extended periods of time. This is an old idea (e.g., Roberts, 1963; Kennicutt, 1983) that has been reformulated in various ways along the years. A updated account is given next.

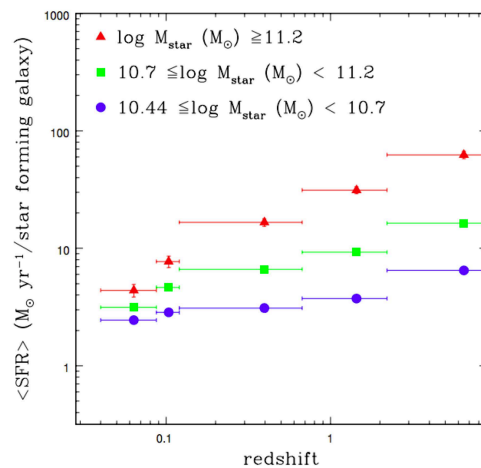


Fig. 2 Observed SFR versus redshift for typical galaxies forming stars at present. The galaxies are divided into three bins according to the present stellar mass (see the inset). Galaxies of all masses have been forming stars over the whole history of the Universe. Figure adapted from Guglielmo et al. (2015, their Fig. 6).

Except for the most massive ones, galaxies have been forming star during the whole life-time of the universe. Figure 2 shows the observed SFR versus redshift for typical disk galaxies forming stars at present. The galaxies have been divided into three bins according to the present stellar mass. The figure shows how their SFR has been declining slightly with time but, overall, galaxies of all masses maintain a significant level of SF along the Hubble time (see also Heavens et al., 2004). If no gas supply is provided, the SF shuts off exponentially with a time-scale of

$$\tau_{in} \simeq 0.75 \text{ Gyr}, \quad (10)$$

where we have plugged into Eq. (2) the values 2 Gyr, 2, and 0.3 for τ_g , η and R , respectively (Sect. 2). Since the SF has been active for much longer, a supply of external gas must have been feeding the SF process in all galaxies.

3.2 Relationship between stellar mass, SFR, and gas metallicity

In two independent papers, Mannucci et al. (2010) and Lara-López et al. (2010) found that the scatter in the well-known mass-metallicity relation correlates with the SFR. Such correlation had been suggested in previous studies (Ellison et al., 2008; Peeples et al., 2009; López-Sánchez, 2010). The fact that galaxies with higher SFR show lower metallicity at a given stellar mass is called fundamental metallicity relation (FMR). Figure 3 shows a recent account of the FMR by Salim et al. (2014). Galaxies are separated into two plots according to their SFR, and the difference is clear: high SFR objects (panel A) have lower metallicity than low SFR objects (panel B).

Neither metal-rich outflows nor the variation of the SF efficiency with M_* explain the FMR. However, the stochastic feeding of the SF process with external metal-poor gas provides a natural explanation. The advent of external gas does not change M_* , but it decreases the mean metallicity of the star-forming gas while simultaneously triggering SF. As time goes on, the SF consumes gas and increases its metallicity, until new metal-poor gas arrives and the cycle re-starts. The process is illustrated in Fig. 4. It contains the temporal variation of the gas mass and metallicity predicted by the toy model in Sect. 1, assuming the gas accretion events to be stochastic. The figure shows how the arrival of gas at a particular time increases the gas mass and thus the SFR (Eq. [3]). This gas accretion event comes with a drop in metallicity. The gas is consumed by the SF, that rises the metallicity in a process that in the long run yields the stationary-state value given in Eq. (9). If a collection of galaxies with similar stellar masses are observed at different phases of the cycle triggered by a gas accretion event, they will show a dispersion in metallicity which anti-correlates with the instantaneous SFR, i.e., they will show the FMR. This explanation was already advanced by Mannucci et al. (2010) and it is generally accepted today.

The FMR has received considerable attention in the literature¹, both from an observational point of view, and from the point of view of its interpretation. Sometimes the claims seem to be contradictory, although the community is reaching a consensus in the sense that (1) the FMR is not an observational artifact, (2) it changes with redshift so that all metallicities decrease with increasing redshift, and (3) it is produced by metal-poor gas accretion triggering SF. The next paragraphs summarize the recent observational and theoretical work on the subject.

Observations of the FMR. The correlation between SFR and metallicity is weaker if systematic errors are taken into account (Telford et al., 2016). The cor-

¹ The discovery papers have about 600 citations in the ADS.

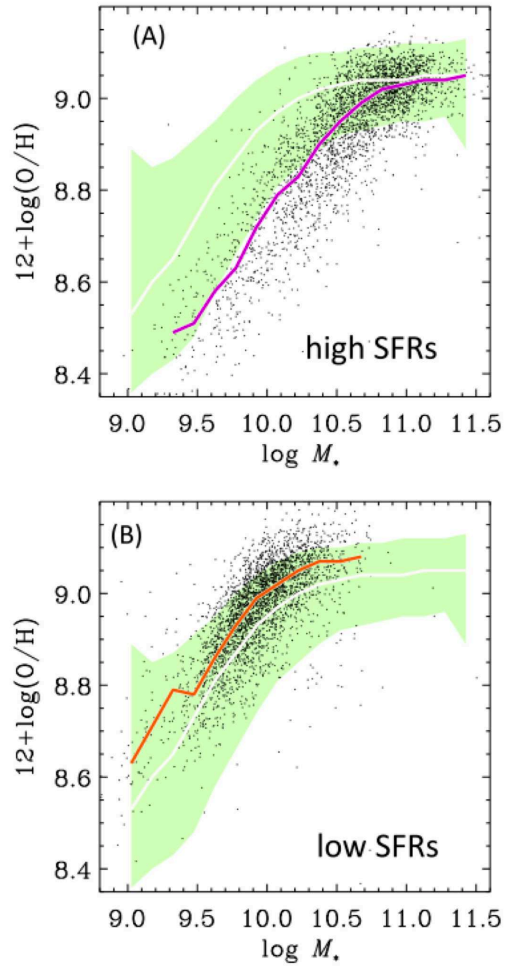


Fig. 3 Gas-phase metallicity versus stellar mass for galaxies with extreme SFR. From a sample of $\sim 250,000$ SDSS objects, the dots in the upper panel (A) show the galaxies with the highest SFRs. The lower panel (B) contains those galaxies with the lowest SFRs. The colored lines represent the median of the distribution of points for a given stellar mass. The green shaded region is the same in (A) and (B) and gives the 90 percentile range of the full sample, with the white line representing the median. Note the systematically lower metallicity for the sample of higher SFR. Figure adapted from Salim et al. (2014).

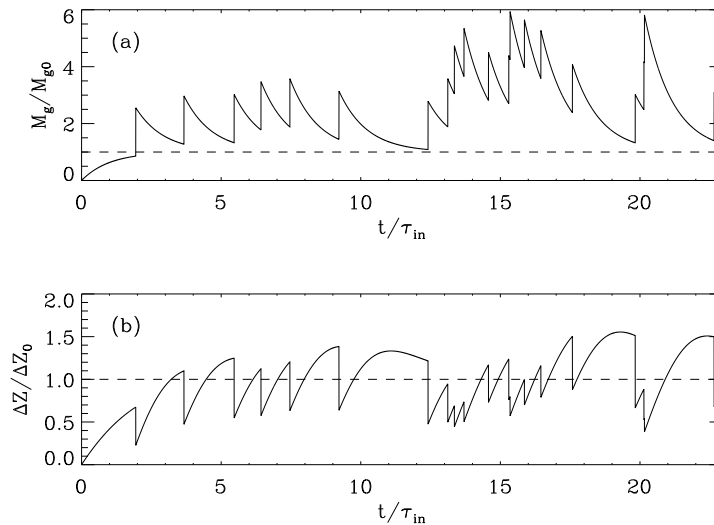


Fig. 4 Variation with time of gas mass (a) and metallicity (b) in a star-forming system where gas clumps are accreted randomly, i.e., at random times and with random masses. Time units are normalized to τ_{in} , the characteristic time-scale for the exponential fall-off of the gas content. The gas of mass and metallicity are normalized to their stationary-state value, indicated by horizontal dashed lines in the figures.

relation may disappear depending on the strong-line ratio used to estimate metallicities (Kashino et al., 2016). The FMR remains even if different metallicity and SFR indicators are used (Salim et al., 2014; Andrews & Martini, 2013).

The FMR disappears when using single H II regions rather than galaxy integrated parameters (Sánchez et al., 2013). There is no FMR in the local star-forming galaxies analyzed by Izotov et al. (2014), whereas it is present in the local sample discussed by Wu et al. (2016). Arguments against the existence of a FMR in star-forming galaxies with redshift smaller than one are presented by Izotov et al. (2015). There is no obvious FMR for galaxies with redshifts between 1 and 2, according to Divoy et al. (2014). There is not relationship at redshift 0.8 (de los Reyes et al., 2015).

At redshift around 1.4, the deviation from the MZR depends on the SFR, so that galaxies with higher SFR show lower metallicities at a given M_* (Yabe et al., 2012). The FMR is still in place at redshift around 0.9, but the metallicities are systematically lower given M_* and SFR (Ly et al., 2014, 2015). Galaxies with younger and more vigorous star formation tend to be more metal poor at a given M_* (redshift between 0.3 and 0.9; Amorín et al., 2014). The FMR is in place at $z \geq 2$ (Cullen et al., 2014). Galaxies at redshift 2 show evidence that the SFR is still a second parameter in the MZR, and are consistent with a non-evolving FMR (Maier et al., 2014). The FMR is in place at redshift 1.6, but it has evolved with respect to the FMR in the

local universe so that metallicities are smaller (Zahid et al., 2014). At redshift 3.4, the metallicity generally anti-correlates with the distribution of SFR and with the gas surface density, although the relation differs from the FMR in the local universe (Troncoso et al., 2014). The evolution of the FMR previously reported in the literature may be an artifact introduced by the use of the different metallicity indicators at different redshifts (Cullen et al., 2014). There is a FMR at redshift 0.7 that seems to agree with the local one (Maier et al., 2015). There is no correlation at redshift 2.3 (Sanders et al., 2015). The FMR evolves with redshift (Brown et al., 2016). There is no significant dependence of the metallicity on SFR at fixed redshift and M_* (objects with redshifts between 0.6 and 2.7; Wuyts et al., 2016).

There is also a *more fundamental* FMR where the SFR is replaced with the gas mass (Bothwell et al., 2013). The scatter of the FMR is reduced if HI mass is used instead of SFR (Jimmy et al., 2015). The central role assigned to the gas mass at the sacrifice of the SFR is also defended by Bothwell et al. (2016a) and Bothwell et al. (2016b). Moreover, Lian et al. (2015) claim that stellar age, rather than SFR or gas mass, is the third parameter in the FMR.

There is a correlation between the metallicity gradient along the radial distance in a galaxy and the SFR, in the sense that galaxies with high SFR tend to show flatter gradient (Stott et al., 2014).

Interpretations of the FMR. Most of the available explanations are based on simple analytical models very much in the spirit of the one described in Sect. 1. For example, Lilly et al. (2013) present a model galaxy whose properties self-regulate due to the short gas depletion time-scale. The model galaxy is near the stationary state, but the gas reservoir available to form stars is allowed to change in time. This drives the system out of the stationary state and provides a dependence of the metallicity on the SFR and mass gas. (The metallicity does not depend on the SFR in the stationary state; see Eq. [9].) The work by Lilly et al. successfully reproduce the FMR, allowing both w and τ_g to vary with stellar mass. It reproduces the overall drop of metallicity with increasing redshift by steadily increasing the gas infall rate. Other works with this type of interpretation are those by Davé et al. (2011), Brisbin & Harwit (2012), Dayal et al. (2013), Forbes et al. (2014b), Pipino et al. (2014), and Harwit & Brisbin (2015). Mergers are also able to reproduce the FMR according to Grønnow et al. (2015).

Dekel & Mandelker (2014) use one of these simple toy models to study the redshift dependence of the FMR, finding problems to reproduce some of the observational constrains, in particular, the ratio SFR/M_g . The need to go beyond simple models because they do not reproduce the observed variation with redshift of SFR/M_g is also argued by Peng & Maiolino (2014).

Yates et al. (2012) use thousands of galaxies from dark-matter numerical simulations to interpret the FMR. Baryons that follow the dark-matter are added, generating a non-stationary clumpy gas accretion that drives the evolution of the model galaxies. The numerical simulation reproduces the main observational trends, including an apparent turnover of the mass-metallicity relationship at very high M_* . The temporal evolution of the gas mass and metallicity of individual galaxies is qualitatively similar to the variations displayed in Fig. 4.

Romeo Velonà et al. (2013) present SPH-cosmological simulations of hundreds of galaxies. Surprisingly, more active galaxies in terms of SFR are also metal-richer (see their Fig. 12). The reason of this contradictory result is not properly understood.

De Rossi et al. (2015) employ hydrodynamical zoom-in cosmological simulations of 500 galaxies to study the scaling relations. The model galaxies show the trends corresponding to the observed FMR. They also find that satellite galaxies have higher metallicity for the same stellar mass, as it is indeed observed (Pasquali et al., 2012).

Kacprzak et al. (2016) find galaxies at redshift around 2 following the FMR. They show that the gas masses and metallicities required to reproduce the observed FMR are consistent with cold-accretion predictions obtained from their hydrodynamical simulations.

3.3 Relationship between lopsidedness and metallicity

Surprisingly, the extremely metal poor (XMP) galaxies of the local universe turn out to show a particular morphology consisting of a bright head and a faint tail, which is commonly referred to as *cometary* or *tadpole*. This correspondence between low metallicity and shape was first noted by Papaderos et al. (2008), and then it has been confirmed in other studies (e.g., Morales-Luis et al., 2011; Filho et al., 2013; Sánchez Almeida et al., 2016). These morphologies represent 80 % of the objects in the XMP catalog used by Filho et al. (2013). The tadpole morphology is not unusual at high redshift, where galaxies tend to be clumpy and elongated (Elmegreen et al., 2005), however it is rather uncommon in the local universe where XMPs reside. For reference, only 0.2 % of the star-forming galaxies in the Kiso survey are cometary (Elmegreen et al., 2012). Figure 5 displays several of these XMP galaxies with the characteristic morphology.

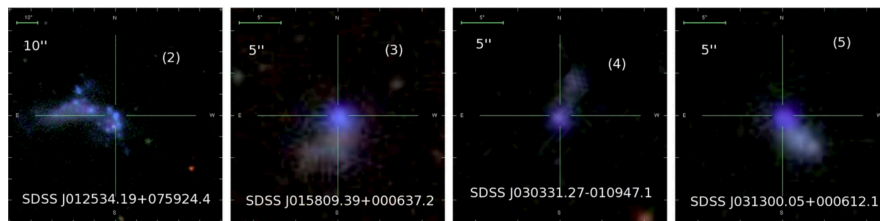


Fig. 5 Typical set of galaxies selected only because they are XMP. Surprisingly, they tend to show cometary or tadpole morphology, with a bright blue head and a faint redder tail. The images are composite color images from SDSS broad-band filters, therefore, they trace stellar light. Adapted from Fig. 5 in Morales-Luis et al. (2011).

Even though XMP galaxies are a very particular type of galaxy, the morphology-metallicity relation that they exhibit is only the extreme case of a common behavior

followed by many star-forming galaxies. Reichard et al. (2009) quantify the lopsidedness of 25,000 star-forming galaxies from SDSS using the amplitude of the $m = 1$ azimuthal Fourier mode. At a fixed mass, the more metal-poor galaxies turn out to be more lopsided, extending the morphology-metallicity relation to the full population of star-forming galaxies.

This property of the XMPs and the other galaxies can be naturally understood within the *gas accretion triggering* scenario. The actual characteristics of the starbursts induced by gas accretion are far from being properly understood and modeled (e.g., Verbeke et al., 2014; Casuso et al., 2006, see also Sect. 4). However, a few general trends seem to be clear. The accreted gas is metal-poor (e.g., Dekel et al., 2009; van de Voort & Schaye, 2012), and it induces off-center giant star-forming clumps that gradually migrate toward the disk centers (Ceverino et al., 2010; Mandelker et al., 2014). The giant star-forming clumps may be born *in-situ* or *ex-situ*. In the first case, the accreted gas builds up the gas reservoir in the disk to a point where disk instabilities set in and trigger SF. In the second case, already formed clumps are incorporated into the disk. They may come with stars and dark matter, and thus, they are often indistinguishable from gas-rich minor mergers (Mandelker et al., 2014). In any case, a significant part of the SF in the disks occurs in these giant clumps. As a result of the whole process, the gas accretion produces bright off-center starbursts increasing the lopsidedness of the host disk. This increase and the decrease of metallicity come hand-to-hand together, giving rise to a relation between morphology and metallicity qualitatively similar to the observed one.

We note, however, that the same trend can also be reproduced by gas-rich metal-poor mergers (e.g. Kazantzidis et al., 2009; Pawlik et al., 2016). As we pointed out above, *gas-rich minor mergers* and *gas accretion events* are often impossible to distinguish, both observationally and from the point of view of the numerical simulations. On the one hand, it is unclear how to define *galaxy* at the low-mass end of the galaxy mass function. If the presence of stars is essential (see Forbes & Kroupa, 2011), whether a gas dominated system is or is not a galaxy ultimately depends on the sensitivity of the observation (e.g., Cannon et al., 2014; Serra et al., 2015; Janowiecki et al., 2015). On the other hand, the presence or absence of stars in a particular dark-matter halo of a numerical simulation depends on details of the assumed sub-grid physics, which may or may not be adequate to describe the formation of stellar systems in objects with sizes and masses at the resolution of the simulation.

This remarkable association between SFR and lopsidedness has been observed in the HI morphology too. Lelli et al. (2014) find that dwarfs with active SF have more asymmetric outer HI envelopes than typical irregulars. Moreover, galaxies hosting an old burst (≥ 100 Myr) have more symmetric HI morphology than those with a young one (≤ 100 Myr).

3.4 Metallicity drops in starbursts of local star-forming galaxies

According to the conventional wisdom, the gas of the local gas-rich dwarf galaxies has uniform metallicity (Kobulnicky & Skillman, 1996; Croxall et al., 2009; Pilyugin et al., 2015). However, there is mounting evidence that some particular objects do show metallicity inhomogeneities (Papaderos et al., 2006; Izotov et al., 2009; Werk et al., 2010; Levesque et al., 2011; Izotov et al., 2012; Haurberg et al., 2013; Sánchez Almeida et al., 2013; Thöne et al., 2014; Sánchez Almeida et al., 2014b; Richards et al., 2014). They are often associated with star-forming regions, so that a drop in metallicity occurs in regions of intense SF.

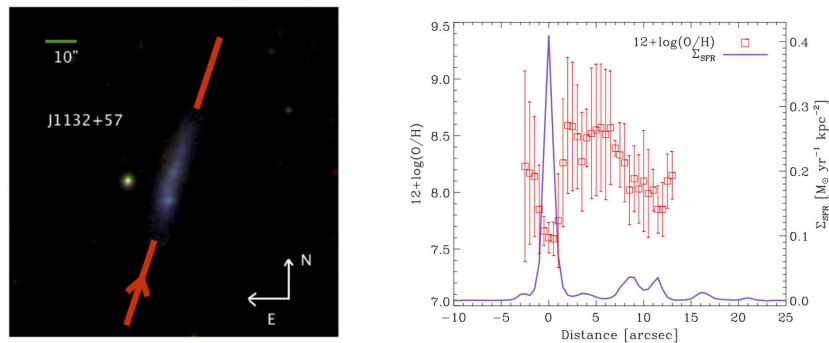


Fig. 6 Left: SDSS image of the XMP galaxy J1132+57, with the red bar indicating the position of the slit during observation. The arrows indicate north and east, and the scale on the top left corner corresponds to 10 arcsec. Right: variation of surface SFR (blue solid line) and oxygen abundance (red symbols with error bars) along the slit. Note the drop in abundance associated with the peak SFR. Figure adapted from Sánchez Almeida et al. (2015).

Sánchez Almeida et al. (2015) carried out a systematic study of the variation of gas metallicity along the major axis of a representative sample of XMP galaxies. Metallicities were inferred using HCM (Pérez-Montero, 2014), a code that compares the observed optical emission lines with photoionization models and which provides metallicity measurements in agreement with direct-method within 0.07 dex. Figure 6 contains the result for one of the galaxies. It shows a clear drop in metallicity at the peak surface SFR. The pattern is the same in 9 out of the 10 studied galaxies. The XMP star-forming clumps are immersed in a host galaxy which is several times more metal-rich. Figure 7 summarizes these results. Independent observations prove that the XMP galaxies rotate, and that the star-forming clumps of low metallicity are dynamically decoupled from the underlying disk (Olmo-García et al., 2016).

The existence of localized metallicity drops suggests a recent metal-poor gas accretion episode. The time-scale for the azimuthal mixing of the gas in turbulent disk is short, of the order of a fraction of the rotational period (e.g., de Avillez & Mac Low, 2002; Yang & Krumholz, 2012; Petit et al., 2015), equivalent to a few hundred Myr. Therefore, the metal-poor gas forming stars must have arrived to the disk recently,

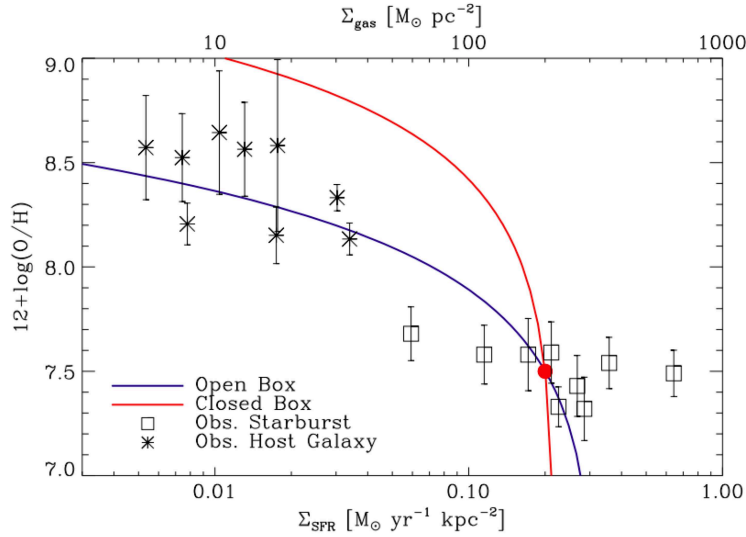


Fig. 7 Summary plot with the oxygen abundance of the starburst (square symbols) and the host galaxy (asterisks) for the XMP galaxies studied by Sánchez Almeida et al. (2015). They are represented versus the surface SFR inferred from $H\alpha$. The star-forming clumps are 0.5 dex metal-poorer than the host, and have a SFR between 10 and 20 times larger. The axis on top gives the gas surface density. The lines show the chemical evolution of a clump at the position of the red bullet depending on whether it evolves as a closed-box (red line) or as an open box (blue line). Taken from Sánchez Almeida et al. (2015).

as naively expected for SF episodes driven by external metal-poor gas accretion. As we discussed in Sect. 3.3, the triggering of SF feeding from external gas is a complex process not properly understood yet (see also Sect. 4). There is a significant degree of gas mixing in the CGM (Sect. 4) and the *naïve* interpretation may not be correct. However, the cosmological numerical simulations of galaxies analyzed by Ceverino et al. (2016) are reassuring. The model galaxies produce off-center star-forming clumps with a metallicity lower than the metallicity of their immediate surroundings. Figure 8, taken from Ceverino et al. (2016), shows metallicity versus surface SFR for a number of clump intra-clump pairs. Each pair is joined by a dotted line. They follow a clear pattern where the point of lower metallicity coincides with the point of larger SFR. Qualitatively, the figure resembles the behavior of the star-forming clumps in XMPs (see Fig. 7).

3.5 The traditional G-dwarf problem

This observation is included here both for historical reasons, and because the accepted interpretation is easy to understand in terms of the toy model described in

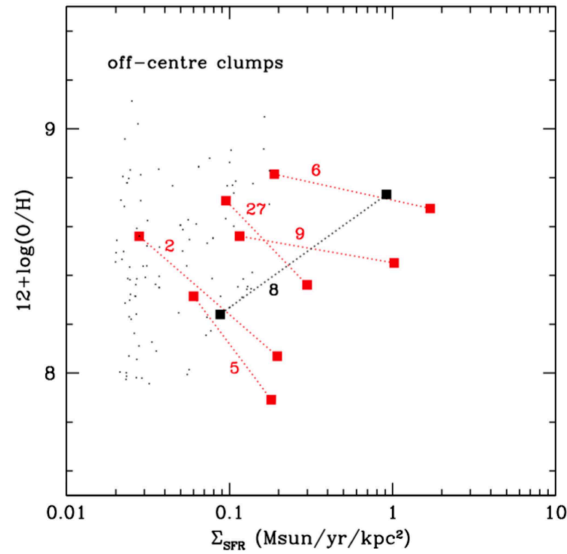


Fig. 8 Metallicity [$12 + \log(\text{O}/\text{H})$] versus surface SFR (Σ_{SFR}) for a number of clumps and their nearby intra-clump medium in the cosmological numerical simulations of galaxies by Ceverino et al. (2016). Each pair is joined by a dotted line. In all but one case (the one shown in black), the region of large SFR (the clump) has lower metallicity than the nearby region of small SFR (the intra-clump medium). The small black dots represent 100 randomly chosen apertures in one of the model galaxies. Adapted from Fig. 3 in Ceverino et al. (2016).

Sect. 1. The so-called *G-dwarf problem* was the first clear indication that an external metal-poor gas supply was needed to explain the observed properties a stellar population.

If a system of pure metal-poor gas evolves as a closed box, each new generation of stars must be less numerous and more metal-rich than the previous one. Therefore, in such a system, the number of stars is expected to decrease with increasing metallicity. However, the distribution of metallicities of the G dwarf stars in the solar neighborhood does not show the fall-off expected in a closed box. There is a deficit of sub-solar metallicity G dwarf stars in the solar neighborhood (van den Bergh, 1962; Schmidt, 1963; Lynden-Bell, 1975) – see Fig. 9. This *problem* has deserved careful attention in the literature, with solutions going from variations of the IMF (Carigi, 1996; Martinelli & Matteucci, 2000) to inhomogeneous chemical evolution and star formation (Malinie et al., 1993). Among them, a continuous metal-poor gas inflow sustaining the formation of the G stars seems be the preferred mechanism (Pagel, 2001; Edmunds, 2005). The explanation was first proposed by Larson (1972), who discovered that the SF maintained by constant metal-poor gas accretion reaches a constant value set only by the stellar yield (see Eq. [9]), which implies a value around the solar metallicity. In the context of this explanation, the apparent deficit of sub-solar metallicity G dwarfs is actually an excess of solar metallicity

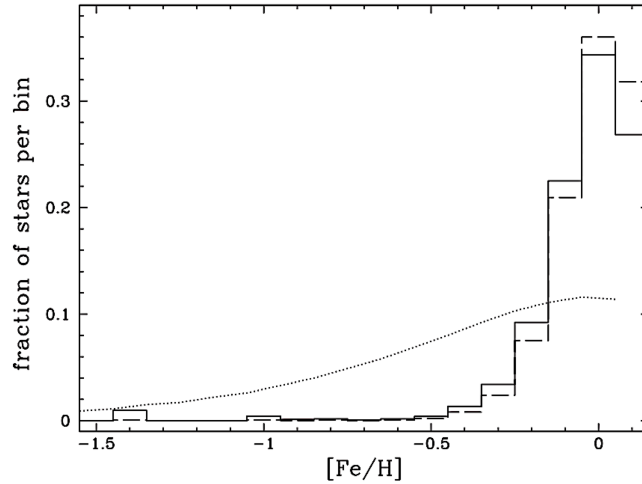


Fig. 9 Fraction of stars in each 0.1 dex metallicity bin. $[\text{Fe}/\text{H}]$ denotes the Fe abundance referred to the solar metallicity in a decimal logarithm scale. The dashed and solid lines represent observed uncorrected and corrected data, respectively. The dotted line is the distribution predicted by a closed-box chemical evolution model, and it largely deviates from the observed one. The observed distribution, from Woolf & West (2012), corresponds to M dwarf stars in the solar neighborhood, but is very similar to the distribution of G dwarfs discussed in the text (see, e.g., Rocha-Pinto & Maciel, 1996).

G dwarf stars formed over time out of an ISM always near equilibrium at approximately the solar metallicity.

The G dwarf problem has also been observed in K dwarfs (e.g., Casuso & Beckman, 2004) and in M dwarfs (e.g., Woolf & West, 2012), and it exists in other galaxies as well (e.g., Worthey et al., 1996). Current chemical evolution models resort to metal-poor gas inflow to reproduce the spatial distribution of stellar metallicities observed in the disk of spirals (e.g., Chiappini et al., 2001; Magrini et al., 2010; Mollá et al., 2016; Pezzulli & Fraternali, 2016). Such gas inflow is needed for the same reasons invoked to solve the G dwarf problem.

3.6 Existence of a minimum metallicity for the star-forming gas

XMPs are defined as galaxies where the gas that produces stars has a metallicity smaller than 10% of the solar metallicity. They turn out to be quite rare. Systematic searches, such as that carried by Sánchez Almeida et al. (2016), render a few hundred objects in catalogs containing of the order of one million galaxies (XMP represent $\ll 0.1\%$ of the known galaxies). Interestingly, their metallicity, and therefore the metallicity of all local galaxies, seems to have a lower limit at around 2%

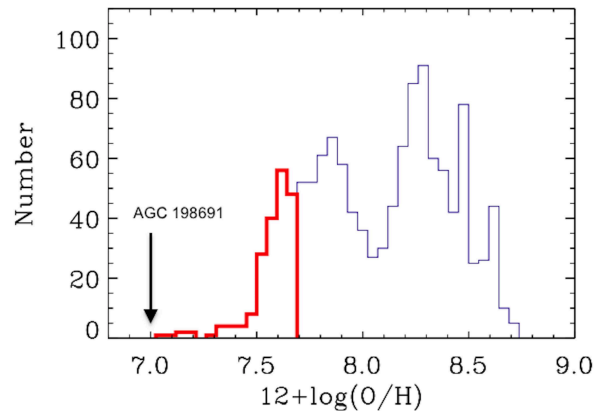


Fig. 10 Distribution of oxygen abundance [$12 + \log(\text{O}/\text{H})$] for all the objects found in the search for low-metallicity galaxies by Sánchez Almeida et al. (2016). The solar metallicity is set at $12 + \log(\text{O}/\text{H})_{\odot} = 8.69$, therefore, the value $12 + \log(\text{O}/\text{H}) = 7.69$ separates the XMPs (the thick red line) and the failed XMP candidates (the thin blue line). There is a clear drop in the distribution towards low metallicity, with no object metal-poorer than 2% of the solar metallicity. AGC 198691 is the star-forming galaxy with the lowest metallicity known (Hirschauer et al., 2016), and the lower limit it sets is marked with an arrow. Figure adapted from Sánchez Almeida et al. (2016).

of the the solar metallicity. Figure 10 displays the distribution of metallicities found by Sánchez Almeida et al. (2016) in the search for XMP candidates in SDSS. It has a sharp cut-off at low metallicity, with no galaxy with $12 + \log(\text{O}/\text{H}) \leq 7.0$. The current record-breaking object is AGC 198691, with a metallicity around 2.1% times the solar metallicity (Hirschauer et al., 2016). It is also included in Fig. 10 for reference.

The existence of this metallicity threshold is not an artifact. Observers have been looking for record-breaking galaxies during the last 45 years, after the discovery of the prototypical XMP galaxy IZw 18 (Sargent & Searle, 1970). These efforts led to enlarging the number of known XMPs (Terlevich et al., 1991; Guseva et al., 2009, 2015; Morales-Luis et al., 2011; Izotov et al., 2012; Sánchez Almeida et al., 2016), but the lower limit metallicity set by IZw 18 remains almost unchanged (the metallicity of IZw 18 is about 3% times the solar metallicity; see, e.g., Thuan & Izotov, 2005).

Several explanations have been put forward to account for the existence of a minimum metallicity in the gas that forms stars. Kunth & Sargent (1986) point out the self-enrichment of the H II region used for measuring. However, the time-scale for the SN ejecta to cool down and mix is of the order of several hundred Myr (e.g., Legrand et al., 2001) and, thus, longer than the age of the H II regions. This fact eliminates the possibility of self-contamination. Self-enrichment by massive star winds seems to be negligible too (Kröger et al., 2006). Kunth & Leboutteiller (2011) suggest the pre-enrichment of the proto-galactic clouds, but it is unclear why

there should be a minimum metallicity for such clouds, except perhaps the value set by the metal contamination produced by Pop III stars. Pop III star contamination has been suggested too (Audouze & Silk, 1995; Thuan & Izotov, 2005), but the expected level of metal enrichment is of the order of 10^{-4} times the solar metallicity (Bromm & Larson, 2004; Muratov et al., 2013), and so much lower than the observed threshold.

Alternatively, if the SF is feeding from gas of the IGM, there is a minimum gas-phase metallicity set by the metallicity of the local IGM. This possibility provides a natural explanation for the long-lasting puzzle. Numerical simulations predict the local cosmic web gas to have a metallicity of the order of 1 % times the solar value (e.g., van de Voort & Schaye, 2012; Rahmati et al., 2016). The metal content of the IGM has been rising over time contaminated by galactic winds, and now it happens to be at the level of the observed metallicity threshold.

Other independent observations also support the existence of a minimum metallicity in the CGM of galaxies at the level of 1 % times the solar metallicity. Lehner et al. (2013) measure the distribution of metallicity of Ly α absorbing clouds around galaxies with redshift up to one. The clouds are observed in absorption against background QSOs. The distribution of metallicity turns out to be bimodal with typical values around 2.5 % solar and 50 % solar. The high-metallicity branch is expected to represent galaxy outflows, whereas the low-metallicity branch corresponds to inflows. The lowest measured metallicity turns out to be 1 % times the solar metallicity. In a completely independent type of work, Filho et al. (2013) studied the HI gas around XMP galaxies. The XMPs happen to be extremely gas-rich, with gas fractions typically in excess of 10. Assuming that all the metals produced by the observed stellar populations have been diluted in their huge HI reservoirs, the metallicity of the HI is again around a few percent of the solar value. The same conclusion has been recently reached by Thuan et al. (2016). Sometimes the metallicity of the HI gas can be measured directly using UV lines in absorption against the stellar light of the galaxy. In the case of IZw 18, Leboutteiller et al. (2013) find that HI region abundances are also around 1 % of the solar value.

3.7 Origin of α -enhanced gas forming stars in local galaxies

The gas forming stars in some of the local dwarf galaxies has elemental abundances which do not scale with the solar abundances. The gas is α -enhanced, using the terminology employed when studying stellar populations in massive galaxies and in the MW halo (e.g., Adibekyan et al., 2011; Vazdekis et al., 2015). The star-forming gas often shows $\log(\text{N}/\text{O}) \simeq -1.5$ (e.g., James et al., 2015; Vincenzo et al., 2016) which is much smaller than the solar value (of the order of -0.86; Asplund et al., 2009). Stars and gas with α -enhanced composition are expected to be formed from the ejecta of young stellar populations (e.g., Izotov & Thuan, 1999), so that low mass stars have not had the time to explode as SN, and so, elements like Fe are underrepresented compared to the solar composition. N is one of these elements,

even though N is also produced in intermediate-mass stars (e.g., Henry et al., 2000). Figure 11 shows the time evolution of N/O in several different model starbursts with very different SF efficiencies (i.e., with different τ_g in the parlance used in Sect. 1). Vincenzo et al. (2016) compute them to model the relationship between N/O and O/H observed in the galaxies of the local universe. Independently of the SF efficiency, when a starburst is 2 Gyr old it has already reached $N/O \simeq N/O_{\odot}$ (see Fig. 11). Something equivalent is shown by Köppen & Hensler (2005) when modeling the evolution of systems that accrete large amounts of metal-free gas. After a transient phase that lasts around 2 Gyr, the system returns to the original N/O_{\odot} . The fact that the gas is α -enhanced is consistent with the thorough study on the heavy element abundances in local star-forming galaxies carried out by Izotov & Thuan (1999). The α -elements Ne, Si, S and Ar, produced by SN explosions of massive ($> 10M_{\odot}$) stars that also produce O, show the same α -element/O ratio as the Sun. However, O turns out to be overabundant with respect to N, C and Fe by factors of around three, which are typical of MW halo stars.

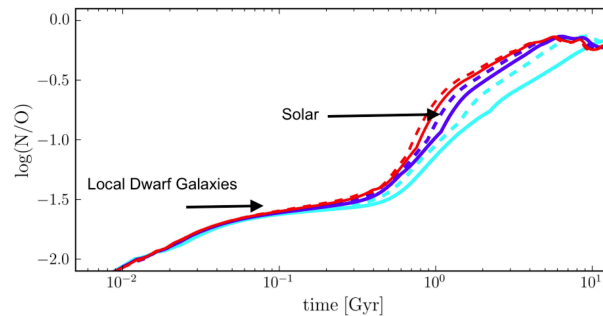


Fig. 11 Time evolution of N/O for chemical evolution models aimed at reproducing the relationship between N/O and O/H exhibited by the galaxies of the local universe. The different curves correspond to different τ_g going from 2 Gyr (solid magenta line) to 0.3 Gyr (red dashed line). The figure includes the N/O found in the Sun and the characteristic value observed in metal-poor galaxies of the local universe. By the time that the burst is 2 Gyr old, N/O has already reached the solar value in all models. Adapted from Vincenzo et al. (2016).

It is well known that all galaxies, including the local dwarf galaxies, have their mass dominated by old stars with ages extending all the way back to the origin of the universe (e.g., Heavens et al., 2004; Sánchez Almeida et al., 2012, see also Fig. 2). The fact that N/O is low in the star-forming gas of some local dwarfs implies that their evolved stellar populations are not the source of the metals. If the metals are not produced by the observed stellar populations, where do they come from? They likely come together with the accreted gas from the IGM. The IGM gas is expected to have α -enhanced chemical composition since the metals it contains were produced by dwarf galaxies in the early universe when the stellar populations were young (e.g., Adelberger et al., 2005; van de Voort & Schaye, 2012; Yates et al., 2013).

The presence of α -enhanced gas forming stars at high redshift seems to be common. Steidel et al. (2016) argue that the unusually high excitation of the gas forming stars in galaxies at redshift around 2 is due to their extreme α -enhanced composition, with $O/Fe \sim 5$ times the solar ratio. Such extreme conditions yield Fe-poor stars in an ISM of moderate-high metallicity as traced by O. Similar physical conditions in the local universe may be responsible for the presence of high excitation narrow He II lines in the spectra of metal-poor galaxies of the local universe (Shirazi & Brinchmann, 2012).

3.8 *The metallicity of the quiescent BCD galaxies*

The blue-compact dwarf (BCD) galaxies are going through an intense starburst phase that cannot be maintained for long. Consequently, there must be many dormant galaxies in a pre or a post BCD phase. They are called quiescent BCDs (QBCD). BCDs possess one or a few bright starburst regions on a low-surface host. Masking out the high-surface knots, Amorín et al. (2007, 2009) characterized the photometric properties of the host galaxy, which likely corresponds to the underlying QBCD. Using these properties as reference, Sánchez Almeida et al. (2008) found out that the SDSS catalog contains as many as 30 QBCDs per BCD. BCDs and QBCDs seem to be drawn from a single galaxy population that metamorphose with a cycle where the quiescent phase lasts 30 times longer than the star-forming phase. However, this interpretation presents a difficulty. The gas metallicity of the QBCDs is systematically higher than the metallicity of the BCDs, which cannot happen if the transformation between QBCD and BCD occurs through closed-box evolution, where the precursor always has lower metallicity than the offspring. The problem naturally goes away if the BCD phase is triggered by the accretion of external metal-poor gas that feeds the observed SF episode. The external driving of the BCD phase also explains why the stellar metallicity of BCDs and QBCDs agrees, even though their gas metallicity differs (Sánchez Almeida et al., 2009). The stellar populations of BCDs and QBCDs are statistically the same because only a small fraction of the galaxy stellar mass is built up in each new burst.

3.9 *Direct measurement of inflows in star-forming galaxies*

To the best of our knowledge, there is no direct measurement of metal-poor gas inflows in the CGM of galaxies. Finding whether a particular Doppler shift corresponds to inflows or outflows is tricky because the same signal is provided by inflows or outflows depending on whether the source is in the foreground or the background. Fortunately, the sense of motion can be disambiguated when the gas is absorbing or emitting against the spectrum of the galaxy. In this cases the gas is in the foreground, which breaks the degeneracy.

Thus, gas inflows have been detected in absorption against stellar spectra (e.g., Rubin & MaNGA Team, 2016), but they are probably associated with metal rich gas returning to the galaxy after being ejected by a starburst or an AGN (e.g., Sancisi et al., 2008; Marasco et al., 2012; Fraternali, 2014). Neutral gas has been studied in absorption in several metal-poor objects (Aloisi et al., 2003; Cannon et al., 2005; Leboutteiller et al., 2009, 2013). However, the relative velocity between the gas absorption and the systemic velocity of the galaxy is too small to tell whether the gas is falling in or going out. If anything, the gas seems to be flowing out with a mild velocity between 10 and 20 km s⁻¹ (Leboutteiller et al., 2013). The origin of this putative metal-poor outflow is puzzling.

Recent observations by Fathivavsari et al. (2016) show signs of infall in DLAs eclipsing QSOs, i.e., dense HI gas so close in redshift to the QSO that it blocks the Ly α emission of the source. Their metallicities are relatively low, and most of them have redshifts larger than that of their background QSO, strengthening the idea that they could be associated with some low metallicity infalling material accreting onto the QSO host galaxies.

Even though the works by Kacprzak et al. (2012, 2015) do not have kinematical information, they are very suggestive of gas inflows in star-forming galaxies. They study the azimuthal distribution of Mg II and O VI absorbers around the galaxy responsible for the absorption. These absorption systems trace gas in the CGM and the IGM, depending on the distance to the galaxy. Kacprzak et al. (2012, 2015) find that the absorption preferentially occurs along the directions pointed out by the minor and the major axes of the central galaxy. The absorbers aligned with the major axis are expected to show gas inflows, with the absorbers in the direction of the minor axis corresponding to gas outflows. In order to secure the whole scenario, one would need to have measurements of the velocity and metallicity of the Mg II systems. Unfortunately, they are not available. However, two independent measurements support the above interpretation. Firstly, outflows prefer the direction perpendicular to the plane of the galaxy because Mg II outflows are faster in face-on galaxies (Bordoloi et al., 2014; Rubin et al., 2014). Secondly, the metallicity of Lyman limit systems (i.e., gas clumps of moderate HI column density) is observed to be bimodal, with one peak at low metallicity and the other at high metallicity (Lehner et al., 2013). This bimodality is to be expected if the observed absorption is produced by metal-poor inflows and metal-rich outflows.

4 Obvious complications and future trends

The evidence discussed in Sect. 3 is all indirect. We have to rely on models to interpret the observables as evidence for gas accretion. The toy model setting up the scene in Sect. 1, and then used in many of the above arguments, oversimplifies many aspects of the accretion process that are important to identify in real galaxies the observational signatures of ongoing cosmological gas accretion. The purpose of this section is to point out some of the obvious complications of a more realistic model-

ing, and also to point out new observational pathways that may reveal connections between SF and the gas of the IGM.

The CGM and the galactic fountain. The CGM is a complex region where gas ejected from the galaxy and gas falling into the galaxy coexist. The gas inflow is not only of cosmological origin. Part of the metal-rich materials ejected in previous SF episodes fall back to the disk in what is called galactic fountain (e.g., Fraternali & Binney, 2006, 2008; Hobbs et al., 2015). The mixing with metal-rich gas from SF processes speeds up the cooling of the hot metal-poor CGM, and the fountain also returns gas that was never ejected (Melioli et al., 2008; Marinacci et al., 2010; Marasco & Fraternali, 2011; Marasco et al., 2012).

The structure of the CGM is extremely complicated according to the current numerical simulations. The morphology of the gas streams becomes increasingly complex at higher resolution, with large coherent flows revealing density and temperature structure at progressively smaller scales, and with no evidence that the substructure is properly captured in the simulations (Nelson et al., 2016). Multiple gas components co-exist at the same radius within the halo, making radially averaged analyses misleading. This is particularly true where the hot quasi-static halo interacts with cold rapidly-inflowing IGM accretion. Some of the resulting complications are revealed in the study of metal-poor DLAs carried out by Yuan & Cen (2016). The majority of the metal-poor DLAs are far from the central galaxy (≥ 20 kpc) and result from the cold gas streams from the IGM. In the migration inwards to the galaxy, they mix up with high-metallicity gas from stellar outflows, removing themselves from the metal-poor category. The change from metal-poor to metal-rich complicates the observational identification of the gas coming from the IGM. IGM gas clouds that get mixed with the CGM and become metal-rich are also found in the simulation by Gritton et al. (2014). The difficulties of interpretation are also put forward by Ford et al. (2014). Using cosmological simulations, Ford et al. examine how HI and metal absorption lines trace the dynamical state of the CGM around low-redshift galaxies. Recycled wind material is preferentially found close to galaxies, and is more dominant in low-mass halos. Typical HI absorbers trace unenriched ambient material that is not participating in the baryon cycle, but stronger HI absorbers arise in cool, metal-enriched inflowing gas. Instantaneous radial velocity measurements are generally poor at distinguishing between inflowing and outflowing gas, except in the case of very recent outflows.

Galactic fountains and metal-rich gas produced in previous starbursts are very important because their presence complicates the search for metal-poor gas inflows in the CGM of galaxies. However, their role in sustaining SF should not be overestimated. Most of the gas used to produce stars at any time is pristine. It was never pre-processed by a star. This issue has been recently quantified by Segers et al. (2016) using galaxies from the EAGLE numerical simulation (Schaye et al., 2015). For MW-like galaxies, recycled stellar ejecta account for only 35 % of the SFR and 20 % of the stellar mass. The contribution was even less important in the past. The toy model in Sect. 1 provides the right order of magnitude for this estimate (see Sánchez Almeida et al., 2014a).

Star formation generated by gas accretion. The current cosmological numerical simulations produce model galaxies that look impressively realistic, and follow most of the well known scaling relations (e.g., Vogelsberger et al., 2014; Schaye et al., 2015). They provide the theoretical framework to understand the formation of galaxies and the role played by cosmological gas accretion in maintaining SF. However, their limited resolution and the dependence of many predictions on the adopted sub-grid physics make them less reliable to study how individual starbursts grow out of the gas that arrives to the galaxy disk. (Predictions on individual star-formation events are discussed in Sec. 3.3.) Improving this aspect is critically important to secure the interpretation of many observables currently used as evidence for cosmological gas accretion.

Imaging the cosmic web. Much of our knowledge on the CGM and IGM comes from observing absorption lines against background sources that happen to be next to galaxies. However, the observation and analysis of these absorption systems is extremely time-consuming, and even the best cases only provide a very sparse sampling of the CGM and IGM around individual galaxies. A complementary approach is observing the cosmic web gas in emission. The mechanisms to produce such emission are varied. $\text{Ly}\alpha$ (as well as $\text{H}\alpha$) can be produced by electron collisions within a gas stream that releases the gravitational energy gained as gas flows from the IGM into the galaxy halo (Dijkstra & Loeb, 2009; Goerdt et al., 2010; Faucher-Giguère et al., 2010). Emission also results from fluorescence induced by an intense UV radiation field such as that produced by a large nearby starburst or a QSO (e.g., Hogan & Weymann, 1987; Cantalupo et al., 2012; Ao et al., 2015).

Radio emission is also expected to trace the cosmic web. In this sense, the search for *dark galaxies* (i.e., objects emitting in 21 cm without optical counterpart) is a very revealing and active field of research (e.g., Cannon et al., 2014; Serra et al., 2015; Janesh et al., 2015; Janowiecki et al., 2015). Gas filaments associated with star-forming galaxies are very interesting too (Sancisi et al., 2008; Lelli et al., 2012; Filho et al., 2013). Radio data easily provide kinematical information, which is so important when investigating flows. In this context, a large filament of molecular gas accreting onto a group of massive high redshift galaxies has been recently discovered by Ginolfi et al. (2016, private communication). This observation is intriguing, but it may open up a new way of addressing the search for IGM gas.

Extremely promising is the recent discovery of an extended $\text{Ly}\alpha$ blob connected to a QSO (Cantalupo et al., 2014). The emission extends beyond the virial radius of the host galaxy so that it traces gas in the IGM. The existence of extended $\text{Ly}\alpha$ emission around QSOs seems to be very common when the observation is deep enough (Borisova et al., 2016). The sensitivity is very much improved using spectrographic observations, which also have the capability of providing the eagerly needed kinematical information (see the chapter by Cantalupo in this Book). Extended $\text{Ly}\alpha$ halos are common around all kinds of galaxies (e.g., Rauch et al., 2016; Momose et al., 2016).

5 Conclusions

Cosmological numerical simulations predict that the SF in regular disk galaxies is feeding from metal-poor gas accreted from the cosmic web. The observational evidence for a relation between SFR and external gas accretion is both numerous and indirect (Sect. 3). One necessarily has to rely on modeling and analysis to identify the existing hints as actual signs of SF driven by metal-poor gas accretion. Thus, the comparison with numerical simulations and a meticulous interpretation of the observations turn out to be mandatory. There is no reason to believe that the magnitude of the problem will change significantly in the near future. The IGM gas is predicted to be tenuous and ionized, and so extremely elusive observationally. The IGM gas gets mixed with metal-rich outflows, and may lose its distinctive metal-poor character to complicate the study. In addition, metal-rich recycled material is also re-accreted, and often velocities are useless to separate inflows from outflows. Although things have much improved during the last few years, theoretical predictions are still very unspecific as far as the details is concerned. These details are needed to interpret particular observational results as evidence for accretion (Sect. 3.4). Finally, the difficulty to distinguish gas accretion events from gas-rich minor mergers confuses the interpretation even further (Sect. 3.3).

Table 1 List of acronyms and symbols defined and used along the text

Acronym	Expansion	Acronym	Expansion
ADS	NASA Astronomical Data System	M_*	Stellar mass
BCD	Blue compact dwarf	M_g	Gas mass
CGM	Circum-galactic medium	QBCD	Quiescent blue compact dwarf
DLA	Damped Lyman- α absorbers	QSO	Quasar
EAGLE	Evolution and Assembly of Galaxies and their Environments Schaye et al. (2015)	SDSS	Sloan Digital Sky Survey
FMR	Fundamental metallicity relation	SF	Star formation
HCM	HII-Chi-Mistry (Pérez-Montero, 2014)	SFR	Star formation rate
IGM	Inter-galactic medium	SN, SNe	Supernova, Supernovae
ISM	Interstellar medium	SPH	Smoothed particle hydrodynamics
IMF	Initial mass function	UV	Ultraviolet
MZR	(Stellar) Mass metallicity relation	w	Mass loading factor (Eq. [4])
MW	Milky Way	XMP	Extremely metal poor
		Z	Metallicity of the gas (Eq. [9])

Acknowledgements Special thanks are due to Casiana Munõz-Tuñón, Debra Elmegreen, and Bruce Elmegreen, for continuous support and for long thoughtful discussions on almost every topic included in the work. I am also indebted to Mercedes Filho, who pointed out many of the references cited in the work, and shared with me her expertise on HI. The interpretative aspects of the work own much to the collaboration with Claudio Dalla Vecchia and Daniel Ceverino. They were always willing discuss the physical aspects of the accretion and the star-formation process. Thanks are due to R. Amorín for the discussions that led to the writing of Sect. 3.7. Thanks are also due to the editors of the Book for giving me the opportunity to contribute, and for their patience

to have my contribution finished. This work has been partly funded by the Spanish Ministry of Economy and Competitiveness, project *Estallidos* AYA2013-47742-C04-02-P.

References

- Adelberger, K. L., Shapley, A. E., Steidel, C. C., et al. 2005, *ApJ*, 629, 636
 Adibekyan, V. Z., Santos, N. C., Sousa, S. G., & Israelian, G. 2011, *A&A*, 535, L11
 Aloisi, A., Savaglio, S., Heckman, T. M., et al. 2003, *ApJ*, 595, 760
 Altay, G., Theuns, T., Schaye, J., Booth, C. M., & Dalla Vecchia, C. 2013, *MNRAS*, 436, 2689
 Amorín, R., Aguerri, J. A. L., Muñoz-Tuñón, C., & Cairós, L. M. 2009, *A&A*, 501, 75
 Amorín, R., Sommariva, V., Castellano, M., et al. 2014, *A&A*, 568, L8
 Amorín, R. O., Muñoz-Tuñón, C., Aguerri, J.A.L., Cairós, L.M., & Caon, N. 2007, *A&A*, 467, 541
 Andrews, B. H. & Martini, P. 2013, *ApJ*, 765, 140
 Ao, Y., Matsuda, Y., Beelen, A., et al. 2015, *A&A*, 581, A132
 Ascasibar, Y., Gavilán, M., Pinto, N., et al. 2015, *MNRAS*, 448, 2126
 Asplund, M., Grevesse, N., Sauval, A. J., & Scott, P. 2009, *ARA&A*, 47, 481
 Audouze, J. & Silk, J. 1995, *ApJ*, 451, L49
 Bigiel, F., Leroy, A., Walter, F., et al. 2008, *AJ*, 136, 2846
 Bordoloi, R., Lilly, S. J., Hardmeier, E., et al. 2014, *ApJ*, 794, 130
 Borisoava, E., Cantalupo, S., Lilly, S. J., et al. 2016, *ApJ*, 831, 39
 Bothwell, M. S., Maiolino, R., Cicone, C., Peng, Y., & Wagg, J. 2016a, *A&A*, 595, A48
 Bothwell, M. S., Maiolino, R., Kennicutt, R., et al. 2013, *MNRAS*, 433, 1425
 Bothwell, M. S., Maiolino, R., Peng, Y., et al. 2016b, *MNRAS*, 455, 1156
 Bouché, N., Dekel, A., Genzel, R., et al. 2010, *ApJ*, 718, 1001
 Bournaud, F., Perret, V., Renaud, F., et al. 2014, *ApJ*, 780, 57
 Brisbin, D. & Harwit, M. 2012, *ApJ*, 750, 142
 Bromm, V. & Larson, R. B. 2004, *ARA&A*, 42, 79
 Brown, J. S., Martini, P., & Andrews, B. H. 2016, *MNRAS*, 458, 1529
 Cannon, J. M., Johnson, M., McQuinn, K. B. W., et al. 2014, *ApJ*, 787, L1
 Cannon, J. M., Skillman, E. D., Sembach, K. R., & Bomans, D. J. 2005, *ApJ*, 618, 247
 Cantalupo, S., Arrigoni-Battaia, F., Prochaska, J. X., Hennawi, J. F., & Madau, P. 2014, *Nature*, 506, 63
 Cantalupo, S., Lilly, S. J., & Haehnelt, M. G. 2012, *MNRAS*, 425, 1992
 Carigi, L. 1996, *RMxAA*, 32
 Casuso, E. & Beckman, J. E. 2004, *A&A*, 419, 181
 Casuso, E., Beckman, J. E., & Buenrostro, V. 2006, *PASP*, 118, 833
 Ceverino, D., Dekel, A., & Bournaud, F. 2010, *MNRAS*, 404, 2151
 Ceverino, D., Sánchez Almeida, J., Muñoz Tuñón, C., et al. 2016, *MNRAS*, 457, 2605
 Chiappini, C., Matteucci, F., & Romano, D. 2001, *ApJ*, 554, 1044
 Christensen, C. R., Davé, R., Governato, F., et al. 2016, *ApJ*, 824, 57
 Croxall, K. V., van Zee, L., Lee, H., et al. 2009, *ApJ*, 705, 723
 Cullen, F., Cirasuolo, M., McLure, R. J., Dunlop, J. S., & Bowler, R. A. A. 2014, *MNRAS*, 440, 2300
 Dalla Vecchia, C. & Schaye, J. 2008, *MNRAS*, 387, 1431
 Dalla Vecchia, C. & Schaye, J. 2012, *MNRAS*, 426, 140
 Davé, R., Finlator, K., & Oppenheimer, B. D. 2011, *MNRAS*, 416, 1354
 Davé, R., Finlator, K., & Oppenheimer, B. D. 2012, *MNRAS*, 421, 98
 Davé, R. and Katz, N. and Oppenheimer, B. D. and Kollmeier, J. A. and Weinberg, D. H. 2013, *MNRAS*, 434, 2645
 Dayal, P., Ferrara, A., & Dunlop, J. S. 2013, *MNRAS*, 430, 2891
 de Avillez, M. A. & Mac Low, M.-M. 2002, *ApJ*, 581, 1047

- de los Reyes, M. A., Ly, C., Lee, J. C., et al. 2015, *AJ*, 149, 79
- De Rossi, M. E., Theuns, T., Font, A. S., & McCarthy, I. G. 2015, *MNRAS*, 452, 486
- Dekel, A., Birnboim, Y., Engel, G., et al. 2009, *Nature*, 457, 451
- Dekel, A. & Mandelker, N. 2014, *MNRAS*, 444, 2071
- Dekel, A., Zolotov, A., Tweed, D., et al. 2013, *MNRAS*, 435, 999
- Dijkstra, M. & Loeb, A. 2009, *MNRAS*, 400, 1109
- Divoy, C., Contini, T., Pérez-Montero, E., et al. 2014, *A&A*, 569, A64
- Edmunds, M. 2005, *Astronomy and Geophysics*, 46, 4.12
- Edmunds, M. G. 1990, *MNRAS*, 246, 678
- Ellison, S. L., Patton, D. R., Simard, L., & McConnachie, A. W. 2008, *ApJ*, 672, L107
- Elmegreen, D. M., Elmegreen, B. G., Rubin, D. S., & Schaffer, M. A. 2005, *ApJ*, 631, 85
- Elmegreen, D. M., Elmegreen, B. G., Sánchez Almeida, J., et al. 2012, *ApJ*, 750, 95
- Fathivavari, H., Petitjean, P., Noterdaeme, P., et al. 2016, *MNRAS*, 461, 1816
- Faucher-Giguère, C.-A., Kereš, D., Dijkstra, M., Hernquist, L., & Zaldarriaga, M. 2010, *ApJ*, 725, 633
- Feldmann, R. 2013, *MNRAS*, 433, 1910
- Filho, M. E., Sánchez Almeida, J., Amorín, R., et al. 2016, *ApJ*, 820, 109
- Filho, M. E., Winkel, B., Sánchez Almeida, J., et al. 2013, *A&A*, 558, A18
- Finlator, K. & Davé, R. 2008, *MNRAS*, 385, 2181
- Forbes, D. A. & Kroupa, P. 2011, *PASA*, 28, 77
- Forbes, J. C., Krumholz, M. R., Burkert, A., & Dekel, A. 2014a, *MNRAS*, 438, 1552
- Forbes, J. C., Krumholz, M. R., Burkert, A., & Dekel, A. 2014b, *MNRAS*, 443, 168
- Ford, A. B., Davé, R., Oppenheimer, B. D., et al. 2014, *MNRAS*, 444, 1260
- Fraternali, F. 2014, in *IAU Symposium*, Vol. 298, Setting the scene for Gaia and LAMOST, ed. S. Feltzing, G. Zhao, N. A. Walton, & P. Whitelock, 228
- Fraternali, F. & Binney, J. J. 2006, *MNRAS*, 366, 449
- Fraternali, F. & Binney, J. J. 2008, *MNRAS*, 386, 935
- Fraternali, F. & Tomassetti, M. 2012, *MNRAS*, 426, 2166
- Genzel, R., Tacconi, L. J., Gracia-Carpio, J., et al. 2010, *MNRAS*, 407, 2091
- Gnedin, N. Y., Tasker, E. J., & Fujimoto, Y. 2014, *ApJ*, 787, L7
- GoerdT, T., Dekel, A., Sternberg, A., et al. 2010, *MNRAS*, 407, 613
- Gritton, J. A., Shelton, R. L., & Kwak, K. 2014, *ApJ*, 795, 99
- Grønnow, A. E., Finlator, K., & Christensen, L. 2015, *MNRAS*, 451, 4005
- Guglielmo, V., Poggianti, B. M., Moretti, A., et al. 2015, *MNRAS*, 450, 2749
- Guseva, N. G., Izotov, Y. I., Fricke, K. J., & Henkel, C. 2015, *A&A*, 579, A11
- Guseva, N. G., Papaderos, P., Meyer, H. T., Izotov, Y. I., & Fricke, K. J. 2009, *A&A*, 505, 63
- Harwit, M. & Brisbin, D. 2015, *ApJ*, 800, 91
- Haurberg, N. C., Rosenberg, J., & Salzer, J. J. 2013, *ApJ*, 765, 66
- Heavens, A., Panter, B., Jimenez, R., & Dunlop, J. 2004, *Nature*, 428, 625
- Henry, R. B. C., Edmunds, M. G., & Köppen, J. 2000, *ApJ*, 541, 660
- Hirschauer, A. S., Salzer, J. J., Skillman, E. D., et al. 2016, *ApJ*, 822, 108
- Hobbs, A., Read, J., & Nicola, A. 2015, *MNRAS*, 452, 3593
- Hogan, C. J. & Weymann, R. J. 1987, *MNRAS*, 225, 1P
- Izotov, Y. I., Guseva, N. G., Fricke, K. J., & Henkel, C. 2014, *A&A*, 561, A33
- Izotov, Y. I., Guseva, N. G., Fricke, K. J., & Henkel, C. 2015, *MNRAS*, 451, 2251
- Izotov, Y. I., Guseva, N. G., Fricke, K. J., & Papaderos, P. 2009, *A&A*, 503, 61
- Izotov, Y. I. & Thuan, T. X. 1999, *ApJ*, 511, 639
- Izotov, Y. I., Thuan, T. X., & Guseva, N. G. 2012, *A&A*, 546, A122
- James, B. L., Kaposov, S., Stark, D. P., et al. 2015, *MNRAS*, 448, 2687
- Janesh, W., Rhode, K. L., Salzer, J. J., et al. 2015, *ApJ*, 811, 35
- Janowiecki, S., Leisman, L., Józsa, G., et al. 2015, *ApJ*, 801, 96
- Jimmy, Tran, K.-V., Saintonge, A., et al. 2015, *ApJ*, 812, 98
- Kacprzak, G. G., Churchill, C. W., & Nielsen, N. M. 2012, *ApJ*, 760, L7

- Kacprzak, G. G., Muzahid, S., Churchill, C. W., Nielsen, N. M., & Charlton, J. C. 2015, *ApJ*, 815, 22
- Kacprzak, G. G., van de Voort, F., Glazebrook, K., et al. 2016, *ApJ*, 826, L11
- Kashino, D., Renzini, A., Silverman, J. D., & Daddi, E. 2016, *ApJ*, 823, L24
- Kazantzidis, S., Zentner, A. R., Kravtsov, A. V., Bullock, J. S., & Debattista, V. P. 2009, *ApJ*, 700, 1896
- Kennicutt, R. C. & Evans, N. J. 2012, *ARA&A*, 50, 531
- Kennicutt, Jr., R. C. 1983, *ApJ*, 272, 54
- Kennicutt, Jr., R. C. 1998, *ApJ*, 498, 541
- Kobulnicky, H. A. & Skillman, E. D. 1996, *ApJ*, 471, 211
- Köppen, J. & Hensler, G. 2005, *A&A*, 434, 531
- Kröger, D., Hensler, G., & Freyer, T. 2006, *A&A*, 450, L5
- Kunth, D. & Leboutteiller, V. 2011, in *EAS Publications Series*, Vol. 48, *EAS Publications Series*, ed. M. Koleva, P. Prugniel, & I. Vauglin, 95–96
- Kunth, D. & Sargent, W. L. W. 1986, *ApJ*, 300, 496
- Lara-López, M. A., Cepa, J., Bongiovanni, A., et al. 2010, *A&A*, 521, L53
- Larson, R. B. 1972, *Nature Physical Science*, 236, 7
- Leboutteiller, V., Heap, S., Hubeny, I., & Kunth, D. 2013, *A&A*, 553, A16
- Leboutteiller, V., Kunth, D., Thuan, T. X., & Désert, J. M. 2009, *A&A*, 494, 915
- Legrand, F., Tenorio-Tagle, G., Silich, S., Kunth, D., & Cerviño, M. 2001, *ApJ*, 560, 630
- Lehner, N., Howk, J. C., Tripp, T. M., et al. 2013, *ApJ*, 770, 138
- Leitner, S. N. & Kravtsov, A. V. 2011, *ApJ*, 734, 48
- Lelli, F., Verheijen, M., & Fraternali, F. 2014, *MNRAS*, 445, 1694
- Lelli, F., Verheijen, M., Fraternali, F., & Sancisi, R. 2012, *A&A*, 537, A72
- Levesque, E. M., Berger, E., Soderberg, A. M., & Chornock, R. 2011, *ApJ*, 739, 23
- Lian, J. H., Li, J. R., Yan, W., & Kong, X. 2015, *MNRAS*, 446, 1449
- Lilly, S. J., Carollo, C. M., Pipino, A., Renzini, A., & Peng, Y. 2013, *ApJ*, 772, 119
- López-Sánchez, Á. R. 2010, *A&A*, 521, A63
- Ly, C., Malkan, M. A., Nagao, T., et al. 2014, *ApJ*, 780, 122
- Ly, C., Rigby, J. R., Cooper, M., & Yan, R. 2015, *ApJ*, 805, 45
- Lynden-Bell, D. 1975, *Vistas in Astronomy*, 19, 299
- Magrini, L., Stanghellini, L., Corbelli, E., Galli, D., & Villaver, E. 2010, *A&A*, 512, A63
- Maier, C., Lilly, S. J., Ziegler, B. L., et al. 2014, *ApJ*, 792, 3
- Maier, C., Ziegler, B. L., Lilly, S. J., et al. 2015, *A&A*, 577, A14
- Malinje, G., Hartmann, D. H., Clayton, D. D., & Mathews, G. J. 1993, *ApJ*, 413, 633
- Mandelker, N., Dekel, A., Ceverino, D., et al. 2014, *MNRAS*, 443, 3675
- Mannucci, F., Cresci, G., Maiolino, R., Marconi, A., & Gnerucci, A. 2010, *MNRAS*, 408, 2115
- Marasco, A. & Fraternali, F. 2011, *A&A*, 525, A134
- Marasco, A., Fraternali, F., & Binney, J. J. 2012, *MNRAS*, 419, 1107
- Marinacci, F., Binney, J., Fraternali, F., et al. 2010, *MNRAS*, 404, 1464
- Martin, C. L. 1999, *ApJ*, 513, 156
- Martin, C. L., Shapley, A. E., Coil, A. L., et al. 2012, *ApJ*, 760, 127
- Martinelli, A. & Matteucci, F. 2000, *A&A*, 353, 269
- Melioli, C., Brighenti, F., D’Ercole, A., & de Gouveia Dal Pino, E. M. 2008, *MNRAS*, 388, 573
- Mollá, M., Díaz, Á. I., Gibson, B. K., Cavichia, O., & López-Sánchez, Á.-R. 2016, *MNRAS*, 462, 1329
- Momose, R., Ouchi, M., Nakajima, K., et al. 2016, *MNRAS*, 457, 2318
- Morales-Luis, A. B., Sánchez Almeida, J., Aguerri, J. A. L., & Muñoz-Tuñón, C. 2011, *ApJ*, 743, 77
- Muratov, A. L., Gnedin, O. Y., Gnedin, N. Y., & Zemp, M. 2013, *ApJ*, 772, 106
- Nelson, D., Genel, S., Pillepich, A., et al. 2016, *MNRAS*, 460, 2881
- Newman, S. F., Genzel, R., Förster-Schreiber, N. M., et al. 2012, *ApJ*, 761, 43
- Olmo-García, A., Sánchez Almeida, J., Muñoz-Tuñón, C., et al. 2016, *ApJ*, submitted
- Pagel, B. E. J. 2001, in *Cosmic evolution*, ed. E. Vangioni-Flam, R. Ferlet, & M. Lemoine, 223

- Papaderos, P., Guseva, N. G., Izotov, Y. I., & Fricke, K. J. 2008, *A&A*, 491, 113
- Papaderos, P., Izotov, Y. I., Guseva, N. G., Thuan, T. X., & Fricke, K. J. 2006, *A&A*, 454, 119
- Pasquali, A., Gallazzi, A., & van den Bosch, F. C. 2012, *MNRAS*, 425, 273
- Pawlik, M. M., Wild, V., Walcher, C. J., et al. 2016, *MNRAS*, 456, 3032
- Peeples, M. S., Pogge, R. W., & Stanek, K. Z. 2009, *ApJ*, 695, 259
- Peeples, M. S. & Shankar, F. 2011, *MNRAS*, 417, 2962
- Peng, Y.-j. & Maiolino, R. 2014, *MNRAS*, 443, 3643
- Pérez-Montero, E. 2014, *MNRAS*, 441, 2663
- Petit, A. C., Krumholz, M. R., Goldbaum, N. J., & Forbes, J. C. 2015, *MNRAS*, 449, 2588
- Pezzulli, G. & Fraternali, F. 2016, *MNRAS*, 455, 2308
- Pilyugin, L. S., Grebel, E. K., & Zinchenko, I. A. 2015, *MNRAS*, 450, 3254
- Pipino, A., Lilly, S. J., & Carollo, C. M. 2014, *MNRAS*, 441, 1444
- Rahmati, A., Schaye, J., Crain, R. A., et al. 2016, *MNRAS*, 459, 310
- Rauch, M., Becker, G. D., & Haehnelt, M. G. 2016, *MNRAS*, 455, 3991
- Reichard, T. A., Heckman, T. M., Rudnick, G., et al. 2009, *ApJ*, 691, 1005
- Richards, S. N., Schaefer, A. L., López-Sánchez, Á. R., et al. 2014, *MNRAS*, 445, 1104
- Roberts, M. S. 1963, *ARA&A*, 1, 149
- Rocha-Pinto, H. J. & Maciel, W. J. 1996, *MNRAS*, 279, 447
- Rodríguez-Puebla, A., Primack, J. R., Behroozi, P., & Faber, S. M. 2016, *MNRAS*, 455, 2592
- Romeo Velonà, A. D., Sommer-Larsen, J., Napolitano, N. R., et al. 2013, *ApJ*, 770, 155
- Rubin, K. & MaNGA Team 2016, *AAS Abstracts*, Vol. 227, 312.10
- Rubin, K. H. R., Prochaska, J. X., Koo, D. C., et al. 2014, *ApJ*, 794, 156
- Salim, S., Lee, J. C., Ly, C., et al. 2014, *ApJ*, 797, 126
- Sánchez, S. F., Rosales-Ortega, F. F., Jungwiert, B., et al. 2013, *A&A*, 554, A58
- Sánchez Almeida, J., Aguerri, J. A. L., Muñoz-Tuñón, C., & Vazdekis, A. 2009, *ApJ*, 698, 1497
- Sánchez Almeida, J., Elmegreen, B. G., Muñoz-Tuñón, C., & Elmegreen, D. M. 2014a, *A&A Rev.*, 22, 71
- Sánchez Almeida, J., Elmegreen, B. G., Muñoz-Tuñón, C., et al. 2015, *ApJ*, 810, L15
- Sánchez Almeida, J., Morales-Luis, A. B., Muñoz-Tuñón, C., et al. 2014b, *ApJ*, 783, 45
- Sánchez Almeida, J., Muñoz-Tuñón, C., Amorín, R., et al. 2008, *ApJ*, 685, 194
- Sánchez Almeida, J., Muñoz-Tuñón, C., Elmegreen, D. M., Elmegreen, B. G., & Méndez-Abreu, J. 2013, *ApJ*, 767, 74
- Sánchez Almeida, J., Pérez-Montero, E., Morales-Luis, A. B., et al. 2016, *ApJ*, 819, 110
- Sánchez Almeida, J., Terlevich, R., Terlevich, E., Cid Fernandes, R., & Morales-Luis, A. B. 2012, *ApJ*, 756, 163
- Sancisi, R., Fraternali, F., Oosterloo, T., & van der Hulst, T. 2008, *A&A Rev.*, 15, 189
- Sanders, R. L., Shapley, A. E., Kriek, M., et al. 2015, *ApJ*, 799, 138
- Sargent, W. L. W. & Searle, L. 1970, *ApJ*, 162, L155
- Schaye, J., Crain, R. A., Bower, R. G., et al. 2015, *MNRAS*, 446, 521
- Schaye, J. & Dalla Vecchia, C. 2008, *MNRAS*, 383, 1210
- Schaye, J., Dalla Vecchia, C., Booth, C. M., et al. 2010, *MNRAS*, 402, 1536
- Schmidt, M. 1959, *ApJ*, 129, 243
- Schmidt, M. 1963, *ApJ*, 137, 758
- Segers, M. C., Crain, R. A., Schaye, J., et al. 2016, *MNRAS*, 456, 1235
- Serra, P., Koribalski, B., Kilborn, V., et al. 2015, *MNRAS*, 452, 2680
- Shen, S., Madau, P., Aguirre, A., et al. 2012, *ApJ*, 760, 50
- Shirazi, M. & Brinchmann, J. 2012, *MNRAS*, 421, 1043
- Silk, J. & Mamon, G. A. 2012, *Research in Astronomy and Astrophysics*, 12, 917
- Skillman, E. D., Kennicutt, R. C., & Hodge, P. W. 1989, *ApJ*, 347, 875
- Somerville, R. S. & Davé, R. 2015, *ARA&A*, 53, 51
- Steidel, C. C., Strom, A. L., Pettini, M., et al. 2016, *ApJ*, 826, 159
- Stott, J. P., Sobral, D., Swinbank, A. M., et al. 2014, *MNRAS*, 443, 2695
- Telford, O. G., Dalcanton, J. J., Skillman, E. D., & Conroy, C. 2016, *ApJ*, 827, 35
- Terlevich, R., Melnick, J., Masegosa, J., Moles, M., & Copetti, M. V. F. 1991, *A&AS*, 91, 285

- Thompson, T. A. & Krumholz, M. R. 2016, *MNRAS*, 455, 334
- Thöne, C. C., Christensen, L., Prochaska, J. X., et al. 2014, *MNRAS*, 441, 2034
- Thuan, T. X., Goehring, K. M., Hibbard, J. E., Izotov, Y. I., & Hunt, L. K. 2016, *MNRAS*
- Thuan, T. X. & Izotov, Y. I. 2005, *ApJS*, 161, 240
- Tinsley, B. M. 1980, *FCPh*, 5, 287
- Tremonti, C. A., Heckman, T. M., Kauffmann, G., et al. 2004, *ApJ*, 613, 898
- Troncoso, P., Maiolino, R., Sommariva, V., et al. 2014, *A&A*, 563, A58
- van de Voort, F. & Schaye, J. 2012, *MNRAS*, 423, 2991
- van den Bergh, S. 1962, *AJ*, 67, 486
- Vazdekis, A., Coelho, P., Cassisi, S., et al. 2015, *MNRAS*, 449, 1177
- Veilleux, S., Cecil, G., & Bland-Hawthorn, J. 2005, *ARA&A*, 43, 769
- Verbeke, R., De Rijcke, S., Koleva, M., et al. 2014, *MNRAS*, 442, 1830
- Vincenzo, F., Belfiore, F., Maiolino, R., Matteucci, F., & Ventura, P. 2016, *MNRAS*, 458, 3466
- Vogelsberger, M., Genel, S., Springel, V., et al. 2014, *MNRAS*, 444, 1518
- Werk, J. K., Putman, M. E., Meurer, G. R., et al. 2010, *ApJ*, 715, 656
- Woolf, V. M. & West, A. A. 2012, *MNRAS*, 422, 1489
- Worthey, G., Dorman, B., & Jones, L. A. 1996, *AJ*, 112, 948
- Wu, Y.-Z., Zhang, S.-N., Zhao, Y.-H., & Zhang, W. 2016, *MNRAS*, 457, 2929
- Wuyts, E., Wisnioski, E., Fossati, M., et al. 2016, *ApJ*, 827, 74
- Yabe, K., Ohta, K., Iwamuro, F., et al. 2012, *PASJ*, 64
- Yang, C.-C. & Krumholz, M. 2012, *ApJ*, 758, 48
- Yates, R. M., Henriques, B., Thomas, P. A., et al. 2013, *MNRAS*, 435, 3500
- Yates, R. M., Kauffmann, G., & Guo, Q. 2012, *MNRAS*, 422, 215
- Yuan, S. & Cen, R. 2016, *MNRAS*, 457, 487
- Zahid, H. J., Kashino, D., Silverman, J. D., et al. 2014, *ApJ*, 792, 75